energies

MDPI

Article

Crosstalk Study of Simultaneous Wireless Power/Information Transmission Based on an LCC Compensation Network

Li Ji [1,2], Lifang Wang [2,3,*], Chenglin Liao [2,3] and Shufan Li [1,2]

1 University of Chinese Academy of Sciences, Beijing 100190, China; jili@mail.iee.ac.cn (L.J.); lishufan@mail.iee.ac.cn (S.L.)
2 Key Laboratory of Power Electronics and Electric Drive, Institute of Electrical Engineering, Chinese Academy of Sciences, Beijing 100190, China; liaocl@mail.iee.ac.cn
3 Beijing Co-Innovation Center for Electric Vehicles, Beijing 100081, China
* Correspondence: wlf@mail.iee.ac.cn; Tel.: +86-10-8254-7090

Academic Editor: K.T. Chau
Received: 23 August 2017; Accepted: 3 October 2017; Published: 13 October 2017

Abstract: The effective simultaneous wireless transmission of power and information (SWTPI) is an issue of great interest. To reduce the crosstalk between power and information channels while increasing the transmission air gap and power level, we introduce an inductor–capacitor–capacitor (LCC) compensation network for an SWTPI system. First, the crosstalk between the power and information channels is analyzed. An effective parametric design method is then proposed for the LCC compensation network, which is analyzed theoretically to minimize the crosstalk. Finally, experiments are conducted at 1000 W and 115.2 kbps with an air gap of 100 cm to verify whether the proposed structure and design method of the LCC compensation network are suitable for the SWTPI.

Keywords: simultaneous transmission of wireless power and information; crosstalk; inductor–capacitor–capacitor (LCC)

1. Introduction

In recent years, wireless power transmission (WPT) technology based on magnetic resonance has developed rapidly in the fields of biomedicine, electronic equipment, electric vehicles, airway transportation and other applications due to not only improvements in the output power and power efficiency of WPT systems, but also the gradual increase in transmission distance [1–7]. However, non-contact charging increases the control complexity. To improve the power and efficiency of WPT systems, feedback information regarding the situation or parameters of the receiver side is urgently needed on the transmitter side [5–11]. Therefore, reliable communication between the transmitter side and the receiver side is essential in WPT systems. The simultaneous wireless transmission of power and information (SWTPI) has been proposed. Many scholars have conducted research in this field, but most current research focuses on small-air-gap and low-power applications. For example, in biomedical applications, several scholars have proposed the use of this approach based on resonance communication technology using two sets of coils to transmit power and information for visual prostheses, artificial hearts and other implant machines [12–16]. The crosstalk between the power and information channels is small due to the low power level, as reported extensively by Junji, Wang and Jiande et al. [16–18]. As the transmission power in an SWTPI system increases, the crosstalk between the energy and information channels reverses the relationship between the transmission power and information rate. For example, several scholars have proposed modulating the data directly on the power carrier via frequency-shift keying (FSK) or amplitude-shift keying (ASK) in the inverter

to transmit power and information synchronously [19,20]. Increasing the energy amplitude will produce significant crosstalk in the data transmission and difficulties in data extraction. Therefore, this method is not suitable for high-power applications. Several papers [17,21–23] have proposed a wireless transmission of power and information (WTPI) structure to transmit power and data in a single inductive link. Thus, the power and data would be transmitted simultaneously through the same pair of coupling coils, and the transmission frequencies of the power and data would deviate significantly from each other in the frequency domain. A rapid signal speed can be achieved because the crosstalk between the power and information channels is small. However, this structure is suitable only for low-power transmission (i.e., less than 1 mW). Based on this structure, a previous work [18] used the series-parallel (SP) compensation network to increase the power level and transmission distance, obtained a crosstalk estimation formula for both sides, and conducted high-power (500 W) and middle-air-gap (12 cm) experiments. However, the crosstalk estimation formula in this structure demonstrated that in a WPT system in which the inductances of the coupled coil and signal coupling inductor are predetermined, the crosstalk between the power and information channels cannot be adjusted. The network will cause significant crosstalk in the information channel as the transmitted power level is improved, further increasing the difficulty of the signal circuit design and reducing the system efficiency because the only way to increase the receiver sensitivity is to improve the transmitted power in the information channel [22]. Therefore, this structure is not suitable for applications that must transmit power exceeding 500 W with air gaps larger than 12 cm. In addition, as the input DC voltage increases, the high-order harmonic crosstalk and switching spike crosstalk in the information channel caused by the inverter cannot be neglected. This issue has been identified [24], but has not been analyzed. Moreover, the high-frequency oscillation in the hard switching process of the inverter will produce considerable crosstalk at the communication frequency, which needs to be avoided in the design of the compensation network. In SWTPI applications with large air gaps (i.e., larger than 12 cm) and high power (i.e., exceeding 500 W), reducing the crosstalk between the power and information channels is a bottleneck.

Recently, a new compensation topology, called the inductor–capacitor–capacitor (LCC) compensation network, has been successfully utilized in stationary and dynamic wireless power charging, particularly in high-power-transmission applications [25–32]. Its advantages in terms of facilitating zero voltage switching (ZVS) of the inverter and improving WPT efficiency under low mutual inductance have been analyzed and demonstrated [18]. Moreover, the current in the transmitting coil is independent of the mutual inductance of the coils, which makes this method suitable for large-air-gap and high-power applications.

This paper proposes a novel structure for the synchronous transmission of wireless power and information in large-air-gap and high-power applications by integrating a double-sided LCC compensation network with the SWTPI structure. The analysis and experiments verify that this structure is suitable for the SWTPI in large-air-gap and high-power applications.

First, the data transmission performance of the proposed structure is analyzed. The results show that the crosstalk based on LCC compensation must be analyzed at the power and communication frequencies, respectively. Then, the crosstalk at the power and communication frequencies is analyzed using an LCC compensation network for the SWTPI. The crosstalk at the communication frequency includes two aspects. The first is the high-order harmonics of the inverter, and the second is the high-frequency content of the switching spike of the switch-on-off process of the inverter. Finally, an effective LCC parameter design method is proposed to minimize the crosstalk. The effectiveness of the design is verified using a system with a transmission power of 1 kW with an air gap of 100 cm and an information transfer speed of 115.2 kbps.

2. Overviews of SWTPI and the LCC Compensation Network

2.1. Overview of SWTPI

The SWTPI is a data transmission method for resonant WPT systems that uses coils and compensation networks originally designed for power transmission [18]. In this method, no additional antennas are required. The communication cell is coupled to the power transfer tank by a transformer or a set of coupled coils. The structure of an SWTPI setup is shown in Figure 1.

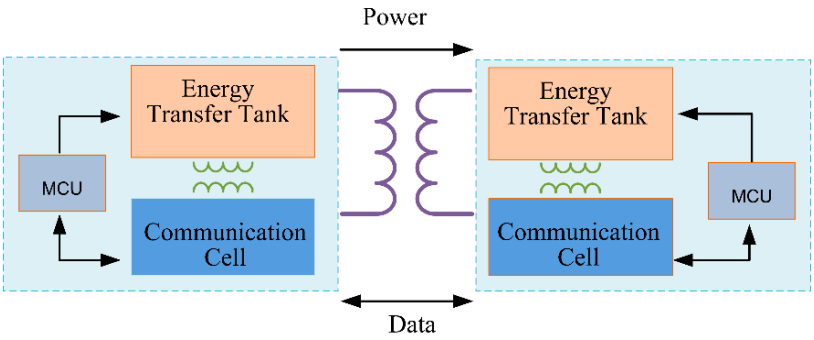

Figure 1. The structure of an simultaneous wireless transmission of power and information (SWTPI) setup.

In this structure, the two tuning points on both sides facilitate data transmission while eliminating extra coils. High-power WPT systems operate at several tens of kHz, and the data-carrier frequency is selected to be at least one order of magnitude higher than the power transfer frequency to minimize crosstalk. The energy transfer tank includes a high-frequency inverter and a compensation network to increase the transfer range. The control strategy of the inverter in the energy transfer tank and the modulation and demodulation methods of the communication cell are all controlled by one microcontroller (MCU). This structure is generally a four-port network, as shown in Figure 2.

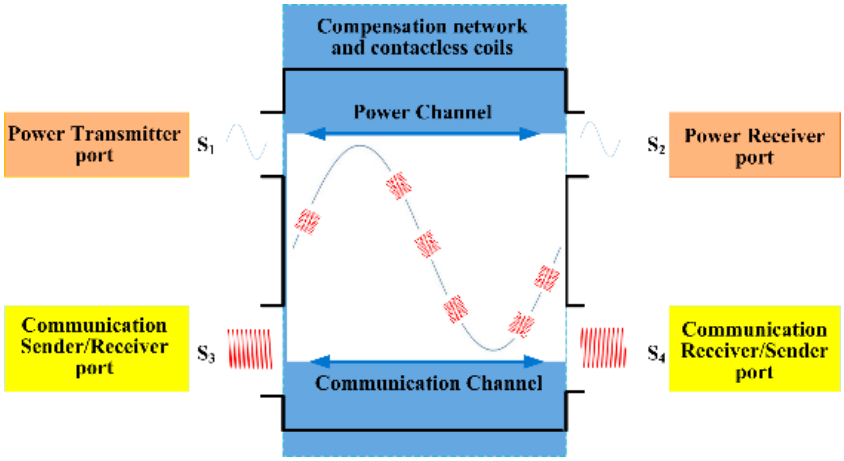

Figure 2. Four-port network diagram for SWTPI.

The blue sine curve represents the energy waveform, the red sinusoid represents the signal waveform, and the two parts of the waveform are superimposed and transmitted by the compensation network and transmission coils. The power is transferred from power port S_1 to power port S_2, and data are exchanged between the data ports S_3 and S_4. The power channel and the data channel reach each port with different transfer functions. The compensation network was originally designed to

transmit resonant power. Therefore, the signal transmission channel is inductive rather than resonant. Clearly, the crosstalk between the power and data channels is influenced by the compensation network, which was designed for power transmission. The primary concern related to power transmission via the SWTPI is increasing the transmission power and efficiency. The most important issue in data transmission by the SWTPI is ensuring the safety of the communication circuit while increasing the signal-to-noise ratio (SNR) to achieve noise immunity.

2.2. Overview of the LCC Compensation Network

The LCC compensation network is a T-type network [26], as shown in Figure 3. The T-type compensation network consists of three ideal, inductive or capacitive hands. In particular, the left and right sides have the same pure inductive reactance of jX, whereas the lower part is purely capacitive and has a reactance of $-jX$.

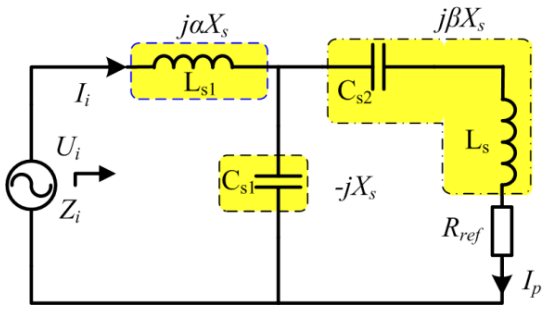

Figure 3. Diagram of the inductor–capacitor–capacitor (LCC) network proposed in [26].

To design the LCC compensation network in practice, the primary current must meet minimum power output requirements, and the ZVS of the inverter should be reached. A perfect T-type network is not the best solution at the primary side to achieve these goals because the equivalent load of the inverter must be somewhat inductive to achieve ZVS. Certain variations [26,28] of the LCC network are needed. One previous work [26] proposed a method that added coefficients α and β to the left and right sides, respectively. As shown in Figure 3, there are two main characteristics of the network for a given impedance R_{ref}:

(1) The overall impedance from the input side becomes

$$Z_i = \frac{jR_{ref}X_S(\alpha-1)+X_S^2(\alpha+\beta-\alpha\beta)}{R_{ref}+jX_S(\beta-1)} \quad (1)$$

(2) Using Equation (1), the output current flowing through R_{ref} can be derived as

$$I_p = \frac{U_i}{-R_{ref}(\alpha-1)+jX_S(\alpha+\beta-\alpha\beta)} \quad (2)$$

3. Crosstalk Study of SWTPI Based on the LCC Compensation Network

3.1. Selection of Compensation Network and Coupling Position

The SWTPI with typical compensation networks are shown in Figure 4. The typical compensation networks are composed of Z_1, Z_2, and Z_3, where Z_1 and Z_2 can be short circuits, capacitors, and/or inductors, and Z_3 can be open circuits, capacitors, and/or inductors [33]. Each side of the WPT system is divided into two loops by the compensation networks. We denote the loop near the energy transmit

and receive coils as loop II and the other one as loop I. Therefore, two positions exist at which the communication cell can be coupled: loop I and loop II.

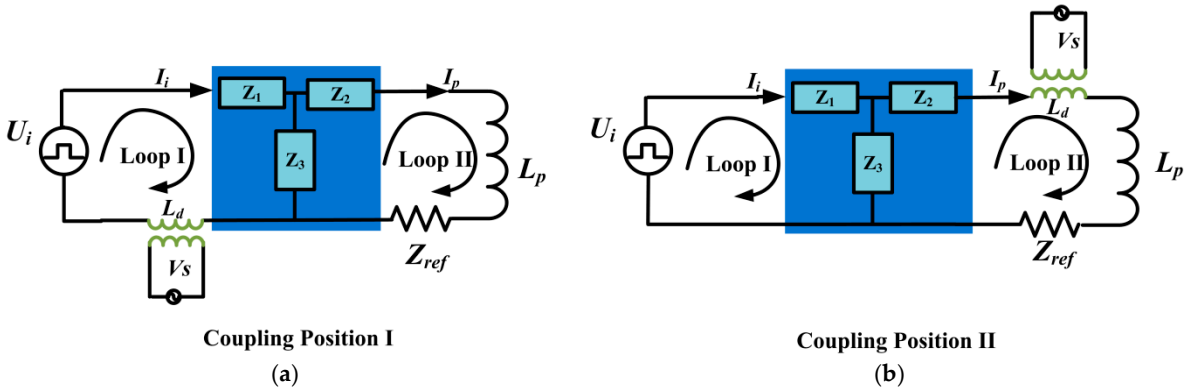

Figure 4. SWTPI structure with different coupling positions. (**a**) Coupling position I; (**b**) Coupling position II.

Given the coupling positions of the signal circuits shown in Figure 4, the voltage of the transmit coil that affects the signal coupling device is deduced as follows:

$$\begin{aligned} U_{L_d}(\omega_p)|_{positionI} &= \frac{Z_3(\omega_p)+Z_2(\omega_p)+Z_{L_p}(\omega_p)+Z_{ref}(\omega_p)}{Z_3(\omega_p)} \cdot \frac{L_d}{L_p} \cdot U_{L_p}(\omega_p) \\ &= \Delta(\omega_p) \cdot \frac{L_d}{L_p} \cdot U_{L_p}(\omega_p) \end{aligned} \tag{3}$$

$$U_{L_d}(\omega_p)|_{positionII} = \frac{L_d}{L_p} \cdot U_{L_p}(\omega_p) \tag{4}$$

$$\Delta(\omega_p) = \frac{Z_3(\omega_p) + Z_2(\omega_p) + Z_{L_p}(\omega_p) + Z_{ref}(\omega_p)}{Z_3(\omega_p)} \tag{5}$$

According to Equations (3) and (4), when $\Delta(\omega_p)$ is less than 1, the cross voltage in L_d at position I will be superior to that at position II. Position II was chosen in a previous work [17–23]. When Z_3 is an open circuit (i.e., when the resonant compensation network is compensated by series resonance), the crosstalk at the two coupling positions is consistent. When Z_3 is not open and is set to parallel resonance with Z_2 and L_p, the crosstalk at coupling position I will change to

$$U_{L_d}(\omega_p)|_{positionI} = \frac{Z_{ref}(\omega_p)}{Z_3(\omega_p)} \cdot \frac{L_d}{L_p} \cdot U_{L_p}(\omega_p) \tag{6}$$

The cross voltage in L_d can be adjusted to be lower than that at coupling position II; that is, because of the different reflected impedance values, the crosstalk can be further reduced by adjusting the values of Z_3 and Z_2.

As the misalignment and distance between the coils increase, the mutual inductance between the coils decreases dynamically. To meet the demand of the charging requirement, the voltage of the transmit coil $U_{Lp}(\omega_p)$ must increase continuously. Thus, the crosstalk at position I is obviously superior to that at position II. The types of compensation networks that are appropriate for coupling position I include LCC, inductor–capacitor–inductor (LCL), and inductor–capacitor (LC) parallel.

Based on the characteristics of constant output current and the ease of realization of ZVS in the LCC resonant compensation network, this paper adopts this compensation network and coupling position I to analyze and minimize the crosstalk.

3.2. Proposed Structure

The proposed structure is shown in Figure 5. This structure consists of seven main parts: the inverter circuit, the signal-sending circuit, the energy-sending compensation network circuit, resonant coils, the energy-receiving compensation network circuit, the signal-receiving circuit, the rectifier circuit and the load. The resonant coils consist of two coils with large inductances: L_s and L_r. The compensation network circuit of the energy transmitter and receiver sides adopts an LCC compensation network circuit that consists of an inductor and two capacitors. The transmitter side includes L_{s1}, C_{s1}, and C_{s2}, and the receiver side includes L_{r1}, C_{r1}, and C_{r2}. The mutual inductance between L_s and L_{s1} and that between L_r and L_{r1} can always be neglected because the values and volumes of L_{s1} and L_{r1} are quite small compared with those of L_s and L_r. The signal-sending circuit consists of a signal source U_s, an impedance-matching capacitor C_{sd1}, a transformer T_s, and a signal source U_s that are coupled to the power channel through the transformer T_s. The information-receiving circuit is composed of a transformer T_r, an impedance-matching capacitor C_{rd} and a receiving resistor R. The transformer T_r and impedance-matching capacitor C_{sd} form a filter that filters out the signal coupled in the power channel. In the proposed method, the data-carrier frequency should be at least one order of magnitude higher than the power frequency to minimize the crosstalk between the power channel and the information channel. Therefore, the resistance and parasitic capacitance of the transformers T_s and T_r cannot be neglected. Thus, the transformers T_s and T_r consist of coupled coils, with coefficients of M_{st} and M_{rt}, resistances of R_{sd1} and R_{sd2} and parasitic capacitances of C_{sd1} and C_{sd2}, respectively. The inductances of T_s and T_r are substantially less than those of L_s and L_r. Therefore, the mutual inductances between T_s and L_s, T_s and L_{s1}, T_r and L_r, and T_r and L_{r1} can be neglected.

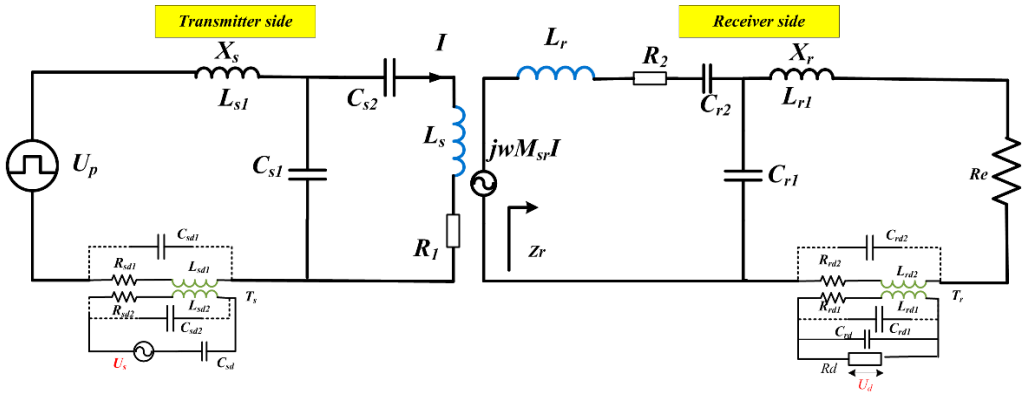

Figure 5. Circuit model of the proposed structure.

In SWTPI systems, the information frequency f_{data} must satisfy the following condition for near-field transmission:

$$airgap << \lambda_{data} = \frac{C}{f_{data}} \tag{7}$$

For an air gap of 1 m, we assume that λ_{data} is 30 m; then, f_{data} will be less than 10 M. To enlarge the air gap, the information frequency must decrease.

3.3. Data Transmission Analysis

As shown in Figure 5, the parameter U_i is the inverter output voltage. The higher-order harmonics in U_i cannot be neglected in large-air-gap and high-power applications. The rectifier with the load is simplified as an equivalent resistance R_e. R_l is the load. The value of R_e is $8R_l/\pi^2$. At the power frequency f_p, the equivalent circuit of communication cells is simplified as an inductor. The transformers T_s and T_r are composed of a set of coupled coils without a terry core, and the coefficient is nearly one. Thus, the core loss of the coupled inductors weakly influences the power

transmission efficiency and overall output power. If the loss of the coupled inductors is ignored, the power delivery performance of the proposed system is similar to that of conventional circuits without communications [28]. L_{sd1} and L_s constitute the left side of the LCC compensation network on the transmitter side, and L_{rd1} and L_r constitute the left side of the LCC compensation network on the receiver side.

Information is transmitted between U_s and U_d. The forward direction is defined as from U_s to U_d, and the backward direction is defined as from U_d and U_s. We will mainly discuss the forward transmission function of the information channel. On the transmitter side of the information channel, the capacitor C_{sd} resonates with L_{sd1}, which is used to amplify the output power of the communication circuit. On the receiver side, the resonant frequency of capacitor C_{rd} and the primary side of transformer T_r are tuned to the data-carrier angular frequency ω_c, and the receiver network works as a narrow band-pass filter to diminish the interference from the power channel. Therefore, the resonant angular frequency ω_c is expressed as:

$$\omega_c = \frac{1}{2\pi\sqrt{L_{sd1} \cdot C_{sd}}} = \frac{1}{2\pi\sqrt{L_{rd1} \cdot C_{rd}}} \tag{8}$$

We ignore parasitic capacitors T_s and T_r because they are too small even at the communication angular frequency ω_d. The impedance of the primary side of transformer T_r is expressed as:

$$Z_{tr1}(\omega) = \frac{1}{1/R_d + 1/(j\omega L_{rd1} + R_{rd1}) + j\omega C_{rd}} \tag{9}$$

The impedance of the secondary side of transformer T_r is expressed as:

$$Z_{tr2}(\omega) = R_{rd2} + j\omega L_{rd2} + \frac{(\omega M_{tr})^2}{Z_{tr1}(\omega)} \tag{10}$$

Thus, the impedance from the receiver side is expressed as:

$$Z_r(\omega) = j\omega L_r + R_2 + \frac{1}{j\omega C_{r2}} + j\omega C_{r1} || (j\omega L_{r1} + R_e + Z_{tr2}(\omega)) = j\omega L_r + R_2 + \frac{1}{j\omega C_{r2}} + \frac{(j\omega L_{r1} + R_e + Z_{tr2}) \cdot (1/j\omega C_{r1})}{j\omega L_{r1} + R_e + Z_{tr2} + 1/j\omega C_{r1}} \tag{11}$$

Using Equation (11), the voltage on L_{rd2} can be derived as:

$$U_{L_{rd2}} = \frac{j\omega L_{rd2} \cdot j\omega M_{sr}}{Z_r(\omega)} \cdot \frac{1/j\omega C_{r1}}{1/j\omega C_{r1} + j\omega L_{r1} + R_e + Z_{tr2}(\omega)} \tag{12}$$

The reflected impedance $Z_{rs}(\omega)$ to the transmitter side is given by:

$$Z_{rs}(\omega) = \frac{(\omega M_{sr})^2}{Z_r(\omega)} \tag{13}$$

The voltage on L_{sd1} can be derived as:

$$U_{L_{sd1}} = j\omega L_{sd1} \cdot \frac{j\omega L_s + 1/j\omega C_{s2} + 1/j\omega C_{s1} + R_1 + Z_{rs}(\omega)}{1/j\omega C_{s1}} \cdot I \tag{14}$$

The transfer functions of the transformers T_s and T_r are:

$$G_{Tr}\omega = \frac{U_d}{U_{L_{rd2}}} = \frac{j\omega L_{rd1} + R_{rd1}}{j\omega L_{rd2}} \tag{15}$$

$$G_{Ts}(\omega) = \frac{U_{L_{sd1}}}{U_s} = \frac{j\omega L_{sd1}}{j\omega L_{sd2} + 1/j\omega C_{sd} + R_{sd2}} \tag{16}$$

The transmission function from the transformer on the receiver side to the transmitter side is defined as:

$$G_{Trs}(\omega) = \frac{U_{L_{rd2}}}{U_{L_{sd2}}} \tag{17}$$

From (8)–(17), the forward transmission function of the information channel is:

$$G_{fc}(\omega) = \frac{U_d}{U_s} = G_{Tr}(\omega) \cdot G_{Ts}(\omega) \cdot G_{Trs}(\omega) \propto M_{sr} \tag{18}$$

From (18), the gain of the forward communication system can be obtained by the Bode diagram by using the data in Table 1, as shown in Figure 6.

Table 1. Parameters used in the prototype.

Parameter	Value
Air gap	100 cm
U_{dc}	210 V
f_p	160 kHz
f_d	6 MHz
L_s, L_r	119 μH, 120 μH
r_{Ls}, rl_{r2}	208 mΩ, 263 mΩ
L_{s1}, L_{r1}	8.36 μH, 7.1 μH
C_{s1}, C_{s2}, C_{r1}, C_{r2}	120 nF, 8.9 nF, 139 nF, 9 nF
L_{sd1}, L_{sd2}, L_{d1}, L_{rd1}	2 μH
r_{sd1}, r_{sd2}, r_{rd1}, r_{rd2}	10 Ω
C_{sd}, C_{rd}	50 pF
M_{sr}	1.98 μH
M_{ts}, M_{tr}	≈2 μH
X_s, X_r	6.97 Ω, 7.14 Ω
R_l	22.4 Ω–30.4 Ω
Misalignment	30 cm
α, β	1.085, 0.932

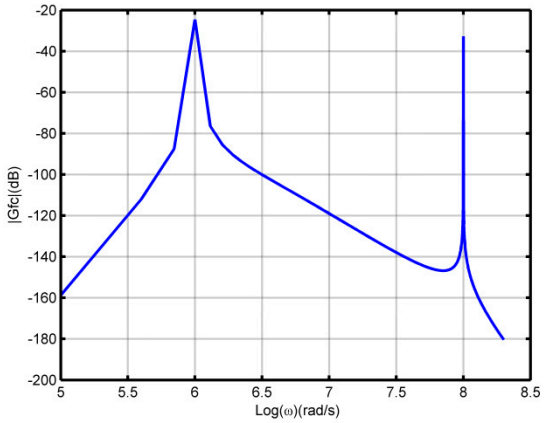

Figure 6. Bode diagram of the forward direction in the information channel.

Figure 6 shows that the system gain at the communication frequency is approximately −30 dB. However, the crosstalk at the power resonant frequency ω_p is approximately −20 dB, which means that in the information channel, there is non-negligible crosstalk at the power resonant frequency ω_p. Apart from that, the high-order harmonic interference for the information channel also cannot be neglected. Although the harmonic voltage is very small, it is not negligible relative to the communication power of −20 dBmW. The power ports are approximately short-circuited at the data-carrier frequency ω_c; thus, the data carrier causes small levels of interference in the power channel. Therefore, it is essential to analyze and minimize the crosstalk from the power channel to the information channel.

3.4. Crosstalk at the Power Frequency Based on the LCC Compensation Network

Previous studies [17,18] have examined the crosstalk at the power frequency with coupling position II. However, the crosstalk estimation formulas in these papers demonstrated that when the inductances of the coupled coil and signal coupling inductor are predetermined, the crosstalk between the power and information channels cannot be adjusted and will increase with the output power at the power frequency, which is not suitable for high-power applications. This paper focuses on coupling position I with the LCC compensation network to minimize the crosstalk at the power frequency by designing the parameters of the LCC compensation network.

To design the LCC compensation network in practice, the primary current must meet minimum power output requirements, and the inverter must achieve Please define abbreviations the first time they appear in the abstract, main body, and a figure or table description. To accomplish these goals, the equivalent load of the inverter needs to be somewhat inductive to ensure that the inverter can achieve ZVS. Certain variations [25,27] of the LCC network are required. A previous paper [25] proposed a method that added coefficients α and β to the left and right sides, respectively, of the LCC compensation network, as shown in Figure 7.

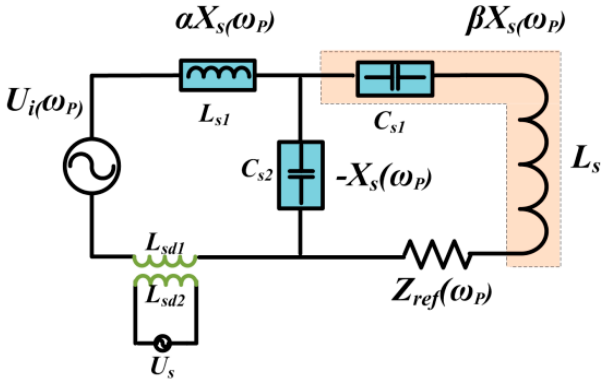

Figure 7. Diagram of the primary side of the proposed SWTPI system at the power frequency.

Therefore,

$$L_{s1} = \frac{\alpha X_s}{j\omega_p} \tag{19}$$

$$C_{s1} = \frac{1}{j\omega_p \cdot (\beta X_s - j\omega_p L_s)} \tag{20}$$

Neglecting the impedance of the transmission coil, the crosstalk at the coupling inductor L_{d1} at the power frequency G_{cs} can be derived as follows:

$$G_{cs}(\omega_p) = \frac{U_{L_{sd1}}}{U_i} = \frac{j\omega L_{sd1}}{\alpha X_s + \frac{-X_s\left(\beta X_s - Z_{ref}\right)}{(\beta-1)X_s + Z_{ref}}} \tag{21}$$

Equation (21) shows that increasing α and decreasing β can decrease the crosstalk at the power frequency, assuming that both the transmission coil and the signal coupling coil are determined.

3.5. Crosstalk at the Communication Frequency Based on the LCC Compensation Network

Since the output waveform of the inverter is square and contains the higher frequency components, the adjacent coupling for the data transmission receives a certain amount of the emitted electromagnetic interference (EMI) noise [17,24]. As the output power and input voltage are improved, the EMI noise will be significantly improved as the harmonic voltage increases at the communication frequency. This part of the noise is the bottom noise of the data transmission; thus, improving the SNR by

minimizing this type of noise is useful. To eliminate noise at other frequencies, we use a band-pass filter on the transmitter side. When the system operates at the communication frequency, the circuit components have parasitic parameters, and the circuit of the primary side is changed to that shown in Figure 8.

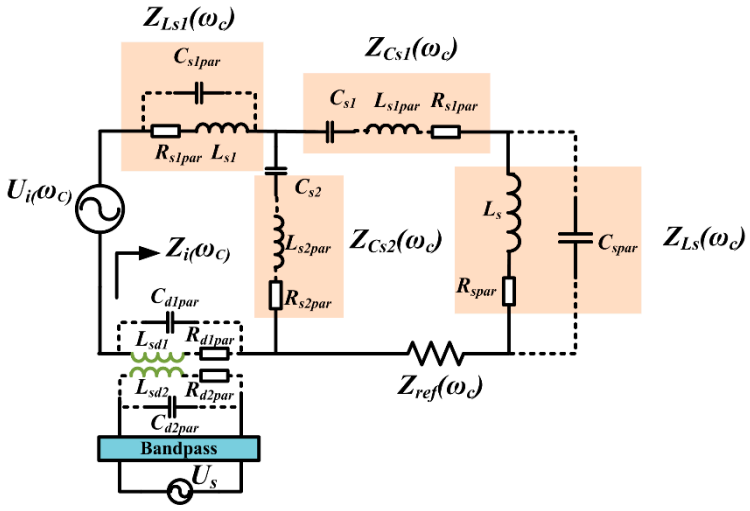

Figure 8. Diagram of the primary side of the proposed SWTPI system at the communication frequency.

Resistor R_{d1par} and capacitor C_{d1par} can be neglected because the inductance of the signal coupling inductor L_{sd1} is very small. C_{s1par}, L_{s1par}, L_{s2par} and C_{spar} can be neglected because these parasitic parameters are sufficiently small at the frequency that satisfies the limitation of (7). Thus, the relationship among the impedances of L_{s1}, C_{s1}, C_{s2}, and L_s at the communication frequency and the power frequency is as follows:

$$\begin{cases} Z_{L_{s1}}(\omega_c) = Z_{L_{s1}}(\omega_p) + R_{L_{s1par}} \\ Z_{C_{s1}}(\omega_c) = Z_{C_{s1}}(\omega_p) + R_{C_{s1par}} \\ Z_{C_{s2}}(\omega_c) = Z_{C_{s2}}(\omega_p) + R_{C_{s2par}} \end{cases} \tag{22}$$

According to the LCC structure described in Section 2.2, we obtain:

$$\begin{cases} Z_{L_{s1}}(\omega_c) = \alpha Z_{C_{s2}}(\omega_c) + R_{L_{s1par}} \\ Z_{C_{s1}}(\omega_c) = \beta Z_{C_{s2}}(\omega_c) + R_{C_{s1par}} \end{cases} \tag{23}$$

Then, the input resistance $Z_i(\omega_c)$ can be derived as:

$$\begin{aligned} Z_i(\omega_c) &= Z_{L_{s1}}(\omega_c) + \left(Z_{L_s}(\omega_c) + Z_{C_{s1}}(\omega_c)\right) || Z_{C_{s2}}(\omega_c) \\ &= \alpha Z_{C_{s2}}(\omega_c) + R_{L_{s1par}} + \left(\beta Z_{C_{s2}}(\omega_c) + R_{C_{s1par}} + Z_{L_s}(\omega_c)\right) || Z_{C_{s2}}(\omega_c) \end{aligned} \tag{24}$$

Assume that $\overline{U_i}(\omega_c)$ is the average voltage of the harmonic of the inverter output voltage that falls within the frequency range of the band-pass filter. Assume that the start and stop angular frequencies of the band-pass filter are ω_a and ω_b, respectively. ω_a and ω_b are determined by the network transmission gain. The value of $\overline{U_i}(\omega_c)$ can be derived as follows:

$$\begin{cases} \overline{U_i}(\omega_c) = \frac{U_i}{\omega_b - \omega_a} = \frac{4U_i}{\sqrt{2}\pi} \cdot \frac{\sum_{k=0}^{(n-m)/2} \frac{1}{m+2k}}{\omega_b - \omega_a} \\ m = \begin{cases} \left\lceil \frac{\omega_a}{\omega_p} \right\rceil, & \left\lceil \frac{\omega_a}{\omega_p} \right\rceil \text{mod} 2 = 1 \\ \left\lceil \frac{\omega_a}{\omega_p} \right\rceil + 1, & \left\lceil \frac{\omega_a}{\omega_p} \right\rceil \text{mod} 2 = 0 \end{cases} \\ n = \begin{cases} \left\lceil \frac{\omega_b}{\omega_p} \right\rceil, & \left\lceil \frac{\omega_b}{\omega_p} \right\rceil \text{mod} 2 = 1 \\ \left\lceil \frac{\omega_b}{\omega_p} \right\rceil - 1, & \left\lceil \frac{\omega_b}{\omega_p} \right\rceil \text{mod} 2 = 0 \end{cases} \\ k \in N \\ \omega_c \in \{\omega_a, \omega_b\} \end{cases} \quad (25)$$

From the circuit diagram and Equations (24) and (25), the crosstalk on the signal coupling inductor L_{sd1} from the power source at the communication frequency can be deduced as:

$$\begin{cases} G_{cs}(\omega_c) = j\omega L_{sd1} \cdot \frac{4U_i}{\sqrt{2}\pi} \cdot \frac{1}{Zi(\omega_c)} \frac{\sum_{k=0}^{(n-m)/2} \frac{1}{m+2k}}{\omega_b - \omega_a} \\ m = \begin{cases} \left\lceil \frac{\omega_a}{\omega_p} \right\rceil, & \left\lceil \frac{\omega_a}{\omega_p} \right\rceil \text{mod} 2 = 1 \\ \left\lceil \frac{\omega_a}{\omega_p} \right\rceil + 1, & \left\lceil \frac{\omega_a}{\omega_p} \right\rceil \text{mod} 2 = 0 \end{cases} \\ n = \begin{cases} \left\lceil \frac{\omega_b}{\omega_p} \right\rceil, & \left\lceil \frac{\omega_b}{\omega_p} \right\rceil \text{mod} 2 = 1 \\ \left\lceil \frac{\omega_b}{\omega_p} \right\rceil - 1, & \left\lceil \frac{\omega_b}{\omega_p} \right\rceil \text{mod} 2 = 0 \end{cases} \\ k \in N \\ \omega_c \in \{\omega_a, \omega_b\} \end{cases} \quad (26)$$

Equations (24) and (26) show that increasing α will help to reduce the crosstalk in the communication frequency.

3.6. Crosstalk from the Switch Process of the Inverter

The data coupling device also receives EMI noise from the switch device due to the hard switch process, which is also part of the adjacent EMI noise [17]. As the output power improves, the switch current and voltage of the switch device will improve significantly, and the EMI noise of this type cannot be neglected. A typical hard switch process of the voltage source inverter is shown in Figure 9. Figure 9a shows waveforms of the voltage and current on the switch in a typical hard switch process. Figure 9b presents the fast fourier transformation (FFT) analysis of the red circle waveform of the current on the switch. Figure 9b shows that when the input voltage is 210 V and the frequency is 160 k, the harmonic voltage at 30 times the baseband is approximately 15 V, which is significant crosstalk for the information channel. To reduce this part of noise, the ZVS of the switch is urgently needed.

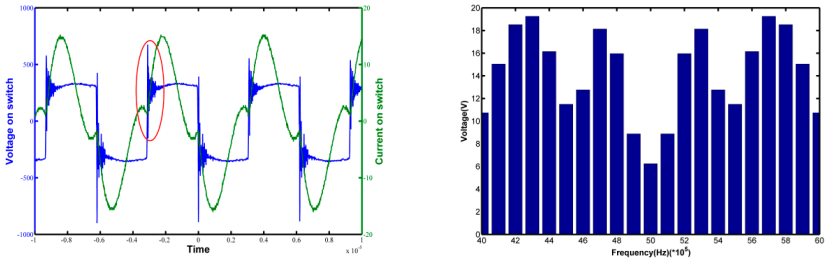

(**a**) (**b**)

Figure 9. Waveforms of the voltage and current on the switch in a typical hard switch process, and fast fourier transformation (FFT) analysis of the red-encircled waveform of the current on the switch. (**a**) Waveforms of the voltage and current on the switch in a typical hard switch process; (**b**) FFT analysis of the red-encircled waveform in (**a**).

3.7. Influence of Misalignment on Crosstalk

The SWTPI system must function under different conditions, including misalignment. Generally, two major misalignment cases show the impact on the coupling coefficients: lateral misalignment and angular misalignment. However, regardless of the type of misalignment, the coupling coefficients between the coils will drop, resulting in variations of R_{ref}. As the coupling coefficient drops, the transmission of the same power will increase the input voltage. As described in Sections 3.3 and 3.4, an increase in the input voltage will introduce more crosstalk not only in the power frequency but also in the communication frequency. Meanwhile, the variations of R_{ref} will change the load situation of the inverter; consequently, the switching process of the inverter will be unable to satisfy the ZVS condition. As described in Section 3.5, failure to satisfy the ZVS condition will introduce more crosstalk at the communication frequency.

4. Crosstalk Minimization via Parameter Design for the LCC Compensation Network

The design method for the receiver side of the LCC compensation network is the same as that described in [25]. Thus, we mainly discuss the design method for the transmitter side of the LCC compensation network. When designing the transmitter side of the LCC compensation network, four aspects must be addressed: (1) minimizing the crosstalk at the power frequency; (2) minimizing the crosstalk at the communication frequency; (3) guaranteeing the current at the primary side to facilitate the transmission of sufficient power; and (4) ensuring that the inverter has ZVS status. We describe the design procedure in detail in the following.

4.1. Minimizing the Crosstalk at the Power Frequency and Communication Frequency

Equation (21) shows that a lower β results in less interference at the power frequency. Therefore, to minimize the interference as much as possible, we assume that the value of β should be less than one.

$$\beta < 1 \tag{27}$$

Equation (26) shows that a larger α results in reduced interference at the communication frequency. Therefore, we assume that the value of α should be greater than one.

$$\alpha > 1 \tag{28}$$

From Equation (2), we can obtain the following:

$$|I_s| = \frac{U_i}{\sqrt{R^2{}_{ref}(\alpha-1)^2 + X^2{}_s(\alpha+\beta-\alpha\beta)^2}} \tag{29}$$

Clearly, when the values of α and β are fixed, the current in the sending coil will decrease with increasing reflection impedance. Therefore, to meet the requirements of power transmission, the current must be greater than or equal to the minimum current requirements in the maximum reflected impedance, i.e.,

$$I_s \geq I_{\text{smin}} = \frac{U_i}{-R_{refMax}(\alpha-1) + jX_s(\alpha+\beta-\alpha\beta)} \tag{30}$$

4.2. Ensuring the ZVS Status of the Inverter

From Equation (1), we can obtain the tangent value of the phase angle θ of Z_i as:

$$\tan\theta = \frac{\text{imag } Z_i}{\text{real } Z_i} = \frac{R_{ref}^2(\alpha-1) - X_s^2(\beta-1)(\alpha+\beta-\alpha\beta)}{R_{ref}X_s} \tag{31}$$

Using Equation (31), we can obtain the derivative of R_{ref} as:

$$\frac{\partial(\tan\theta)}{\partial(R_{ref})} = \frac{(\alpha-1)}{X_s} + \frac{X_s(\beta-1)(\alpha+\beta-\alpha\beta)}{R^2{}_{ref}} \tag{32}$$

Since the value of α is approximately one and X_s is always approximately ten or more ohms, the value of $(\alpha-1)/X_s$ is quite small and weakly influences the value of (32). Thus, $(\alpha-1)/X_s$ can be neglected. Therefore, we obtain:

$$\frac{\partial(\tan\theta)}{\partial(R_{ref})} \approx \frac{X_s(\beta-1)(\alpha+\beta-\alpha\beta)}{R^2{}_{ref}} \tag{33}$$

The contours of Equation (33) are shown in Figure 10. As denoted by the orange ellipse, when $\beta < 1$, Equation (33) is less than zero, which means that the value of $tg\theta$ is a decreasing function of the reflected impedance R_{ref}.

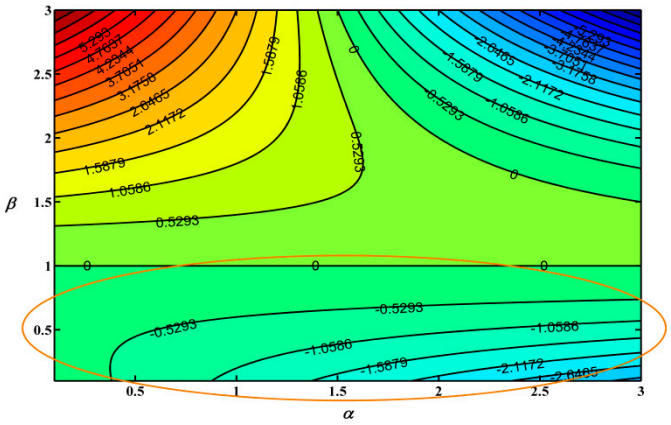

Figure 10. Contour plot of Equation (33).

To ensure the stable operation of the inverter, it is necessary to ensure that the reflection impedance angle is greater than a certain amount at the time of the maximum reflection impedance, i.e.,

$$\tan\theta \geq (\tan\theta)_{\min} = \frac{R^2_{ref\max}(\alpha-1) - X_s^2(\beta-1)(\alpha+\beta-\alpha\beta)}{R_{ref\max}X_s} \tag{34}$$

4.3. Parameter Design Method for the LCC Compensation Network to Minimize the Crosstalk

Using Equations (27), (28), (30), and (34) simultaneously, we obtain:

$$\begin{cases} I_s \geq I_{s\min} = \frac{U_i}{-R_{refMax}(\alpha-1)+jX_s(\alpha+\beta-\alpha\beta)} \\ \tan\theta \geq (\tan\theta)_{\min} = \frac{R^2_{ref\max}(\alpha-1)-X_s^2(\beta-1)(\alpha+\beta-\alpha\beta)}{R_{ref\max}X_s} \\ \beta < 1 \\ \alpha > 1 \end{cases} \tag{35}$$

Using the values in Table 1, we assume that the minimum current needed is 29.8 A and that the minimum reflection angle of impedance is 10°. Then, by solving Equation (35), we can obtain a set of solutions, as shown by the circle in Figure 11.

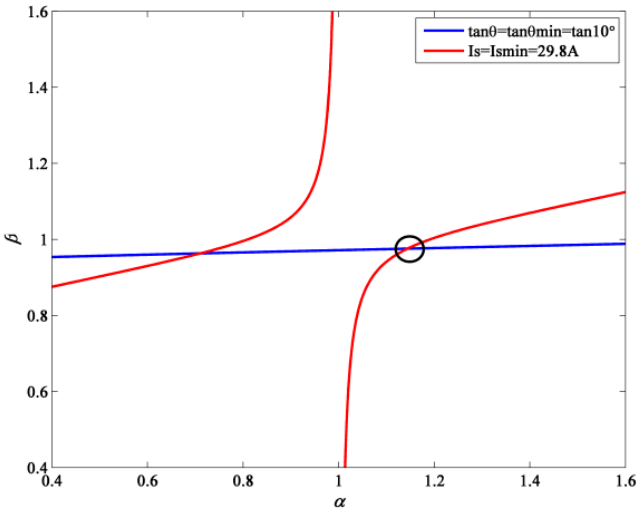

Figure 11. Solutions of Equation (35). U_i = 210 V, X_s = 7 Ω. The maximum value of R_{ref} is 3.6 Ω, and the minimum value of R_{ref} is 1.8 Ω.

The estimated efficiency from the transmit coil to the load is denoted by η_e, and the output power of the system is denoted by P_o. After determining α and β, the parameters of the LCC compensation network on the transmitter side can be calculated using Equation (36):

$$\begin{cases} X_s = \frac{U_i}{I_{rq}} = \sqrt{\frac{8U_{dc}^2 R_{ref}\eta_e}{\pi^2 P_o}} \\ L_{s1} = \frac{\alpha X_s}{\omega} - L_{sd1} \\ C_{s1} = \frac{1}{X_s\omega} \\ C_{s2} = \frac{1}{(\alpha-\beta)\omega X_s} \end{cases} \quad (36)$$

5. Prototype Design and Experimental Validation

5.1. Experimental Set

A 1000-W prototype was built to verify the proposed structure and design method for the LCC compensation network. The parameters are listed in Table 1. Figure 12 shows a photograph of the prototype of our system.

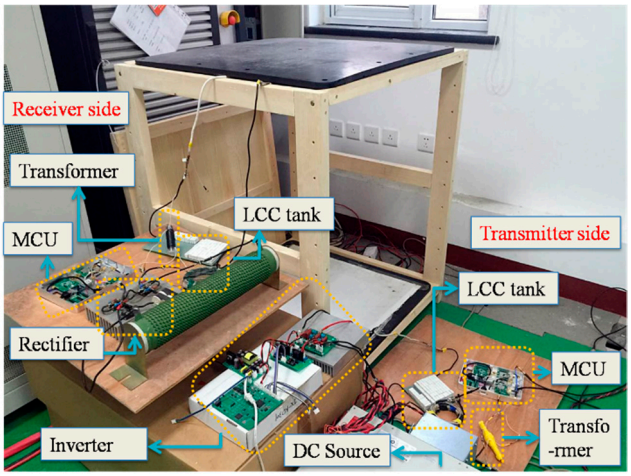

Figure 12. Photograph of our system.

The transmitter side and the receiver side are controlled independently by MPC5674F MCUs (NXP, Netherlands), which regulate the power and data transmission. The size of the power transmitting and receiving coils is 72 × 72 cm, with a turn number of 12. The coil-to-coil wireless charging distance of the prototype is 100 cm. The transmitting coil and the receiving coil have a set of LCC compensation networks, which are encircled and marked. The mutual inductance M between the transmitter and receiver sides is 1.98 μH and is measured by an inductance–capacitance–resistance (LCR) meter. For the transformers T_s and T_r, the inductance of the primary and secondary sides is approximately 2 μH, and the coupling coefficient is 0.98. Considering that the primary side will pass a high current, the transformers T_s and T_r are built with Litz wire.

According to the method for calculating the optimal impedance [25], the optimal impedance of our system is 2.28 Ω. Considering the approximation of the turn-off current for the LCC-connected inverter proposed in [29], the expected impedance angle θ needed to ensure ZVS is calculated as 10°. Thus, according to the maximum and minimum reflection impedances of the system and the limitation of the current in the transmitting coil and the reflection impedance angle, we set the minimum current in the transmitting coil to 29.8 A. By solving Equation (35), we can obtain one set of α and β that can satisfy the requirements, as listed in Table 1.

The transmission gain at the communication frequency in this system is measured by an Agilent N9000B (Keysight, CA, USA) frequency analyzer machine. The transmission gain between 5.6 MHz and 6.9 MHz is above −50 dB, as shown in Figure 13. The peak transmission gain is approximately −30 dB, which is consistent with the simulation result given in Figure 6. Therefore, we choose 6 MHz as the baseband frequency for our information channel. Additionally, this frequency satisfies Equation (7). Thus, ω_a is set to 5.6 MHz, and ω_b is set to 6.9 MHz; the bandwidth is 1.3 MHz.

To obtain the lowest filtering noise, we designed a five-stage band-pass filter on the transmitter side and receiver side in the information channel (Figure 14). Our system uses a UM402 (Cygran, Beijing, China) modulation and demodulation module, and a mixer machine is used to generate the 6-MHz baseband signal.

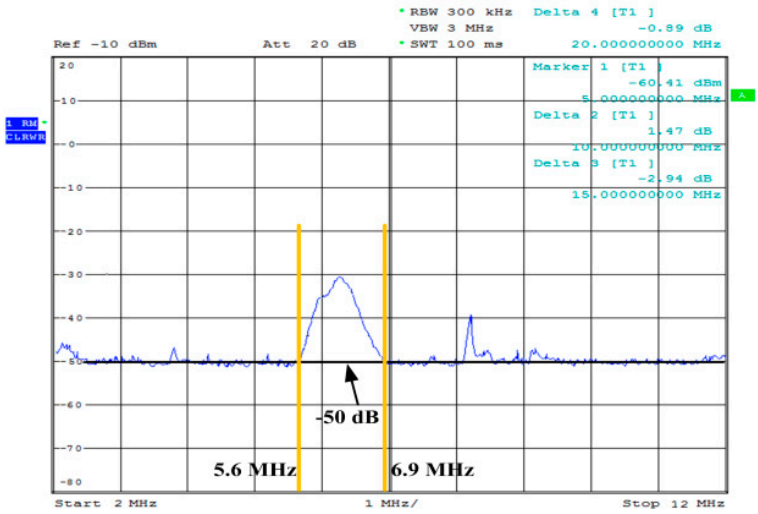

Figure 13. Photograph of the transmission gain at the communication frequency.

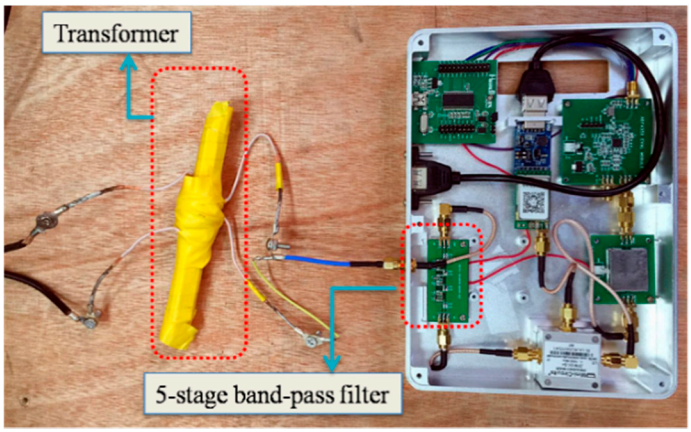

Figure 14. Photograph of the five-stage band-pass filter and transformer.

5.2. Experimental Results

We designed our experiment according to the parameters in Table 1. For the selection of α and β, both the transmission ability and crosstalk were studied to verify the aforementioned analysis.

To verify the effectiveness of the proposed structure and parameter design method, an SWTPI system with coupling position II, which was chosen in previous works [17–23], was built for comparison. The voltages on the main transmitting coil and transformer coil at the power transmission frequency ω_p are listed in Table 2 and are based on the experimental data. The average crosstalk values on the transmitter and receiver sides between the power channel and the information channel at the power transmission angular frequency ω_p were calculated using Equation (21) and are shown in Figure 15.

Table 2. Voltages measured at the power frequency.

Parameter	Value (Avg)
V_s	3150 V
V_{sd1}(*Proposed*)	14.5 V
V_{sd1}(*Previous*)	52.5 V
V_r	3048 V
V_{rd1}(*Proposed*)	1.83 V
V_{rd1}(*Previous*)	50.8 V

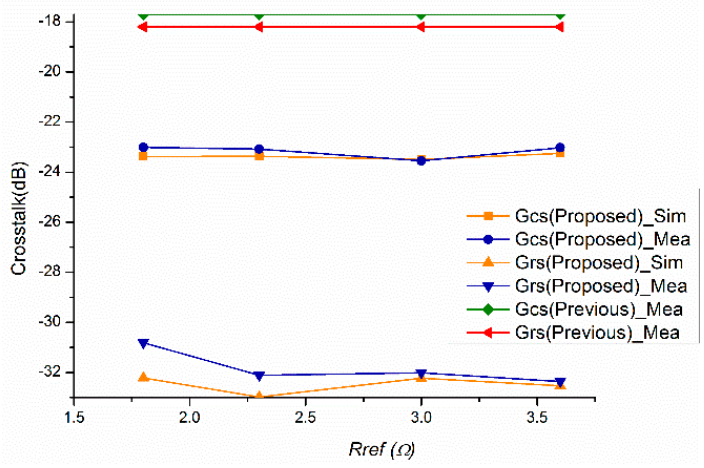

Figure 15. Simulation and measurement of the crosstalk on the transmitter and receiver sides based on the proposed and previous structures for different reflected resistances.

Figure 15 shows the measured and simulated crosstalk at the power frequency based on the proposed and previous structures for different reflected resistances. As shown in Figure 15, the crosstalk based on the proposed structure and design methods is far less than that of earlier works.

At the communication frequency, the crosstalk is decreased by 2 dB using the method described in Section 4. Additionally, the send power of the information channel requires only an average of −20 dBmW, as shown in Table 3.

Table 3. Results obtained at the communication frequency.

Reflected Load	Power In	Power Received	SNR
1.8 Ω	−20 dBmW	−35 dBmW	9 dB
2.3 Ω	−22 dBmW	−32 dBmW	10 dB
3 Ω	−19 dBmW	−30 dBmW	10 dB
3.6 Ω	−21 dBmW	−33 dBmW	11 dB

Moreover, the output current, voltage of the inverter and coil currents under the maximum and minimum reflected resistances were measured, and ZVS was achieved under different reflected resistances, as shown in Figure 16. The average output power of the proposed SWTPI system is 1 kW, and the efficiency is 72.9%.

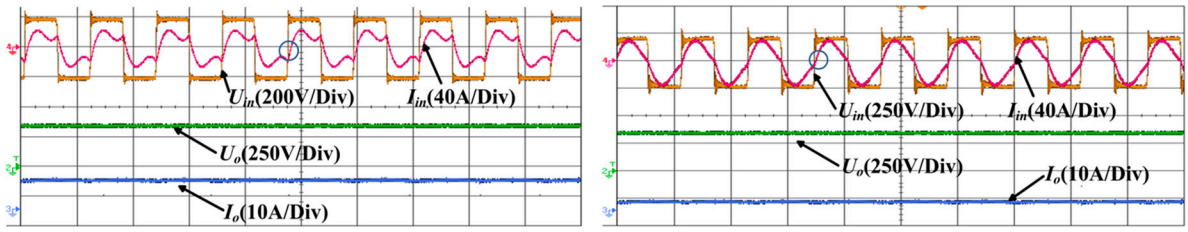

Figure 16. Under maximum R_{ref} and minimum R_{ref} conditions, the measured waveforms of the transmit coil current and the output current, output voltage, and θ of the inverter, with α = 1.085 and β = 0.932. (**a**) Waveforms with R_{ref} = 1.8 Ω, θ = 11°, and I = 29.9 A; (**b**) Waveforms with R_{ref} = 3.6 Ω, θ = 10°, and I = 29.8 A.

Based on Shannon's law, the max communication capacity is defined as [21]:

$$C_{\max} = Bw \log 2(1 + \frac{P_s}{P_p}) \tag{37}$$

Ps is the power of the signal, and *Pp* is the power of the crosstalk. According to the aforementioned bandwidth and the crosstalk, the maximum capacity of this system is 4.5 Mbps. However, because of the experimental limitations, at present the data rate is only 115.2 kbps. However, generally speaking, 115.2 kbps is sufficient to meet the requirements for the transmission of the required information, including location information and information such as start or stop. Figure 17 shows the waveforms on the transmitter and receiver sides at a data rate of 115.2 kbps obtained using the FSK modulate and demodulate methods. The upper part of Figure 17a is the bit stream sent by transmitter, and the lower part of Figure 17a is the waveform in the signal coupling inductor at the transmitter side. The upper part of Figure 17b is the waveform in the signal coupling inductor at the receiver side, and the lower part of Figure 17b is the bit stream received.

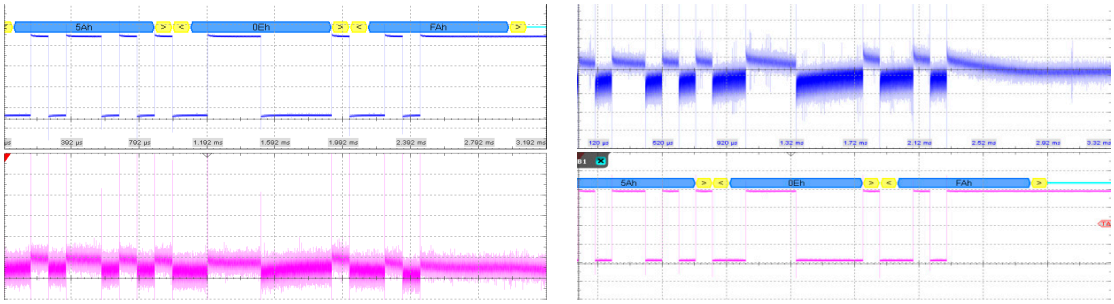

(**a**) (**b**)

Figure 17. Communication waveforms on the transmitter and receiver sides after amplification. (**a**) On the transmitter side; (**b**) On the receiver side.

The transmission abilities of the power and information channels are improved by properly designing the parameters of the compensation network. In addition, the security of the communication in our SWTPI system is improved by decreasing the transmitted communication power.

6. Conclusions

SWPTI between the transmitter side and the receiver side is important in WPT systems. To minimize the crosstalk between the power channel and the information channel, this paper applied an LCC compensation network to an SWTPI system. First, the transmission and crosstalk of the proposed structure were studied. An effective parametric design method of the LCC compensation network for the SWTPI system was then described and analyzed theoretically, with a focus on the power and data transmission abilities and on minimizing the crosstalk at both the power and communication frequencies. A set of LCC networks was designed based on the proposed parametric design method, and the system performances at different loads and misalignments were compared. The crosstalk on the transmitter side and the receiver side decreased by 5 dB and 15 dB, respectively, at the power frequency, and by 2 dB at the communication frequency, compared to previous studies. The average output power and data transmission speed of our SWTPI system were measured to be 1 kW and 115.2 kbps, respectively. Highly consistent measurements between the theoretical analyses and simulation were achieved. In the future, we will further improve the power level and introduce the SWTPI to actual applications, such as electric vehicle wireless charging applications, including stationary and dynamic charging applications. In such applications, the standard output power level is 3.3 kW or 7.7 kW. We will further optimize the circuit parameters to reduce the crosstalk at these power levels. In the meantime, we will improve the anti-crosstalk ability of the information channel by adopting other transmission methods, such as Quadrature Phase Shift Keying (QPSK) and spread spectrum communication. By reducing the crosstalk in the power channel and improving the anti-crosstalk ability of the information channel, the overall system power transmission level and communication rate will ultimately be improved.

Acknowledgments: Authors are gratefully acknowledging the support by Chinese National High-tech R&D (863 program) Project (2015AA016202).

Author Contributions: Li Ji constructed crosstalk models and analyzed parameter design methods. Li Ji and Shufan Li carried out the simulations and experiments. All the authors carried out the data analysis, discussed the results, and contributed to writing the paper.

Conflicts of Interest: The authors declare no conflict of interest.

References

1. Li, S.Q.; Mi, C.C. Wireless Power Transfer for Electric Vehicle Applications. *IEEE J. Emerg. Sel. Top. Power Electron.* **2015**, *3*, 4–17.
2. Choi, S.Y.; Gu, B.W.; Jeong, S.Y.; Rim, C.T. Advances in Wireless Power Transfer Systems for Roadway-Powered Electric Vehicles. *IEEE J. Emerg. Sel. Top. Power Electron.* **2015**, *3*, 18–36. [CrossRef]
3. Chopra, S.; Bauer, P. Driving Range Extension of EV with On-Road Contactless Power Transfer-A Case Study. *IEEE Trans. Ind. Electron.* **2013**, *60*, 329–338. [CrossRef]
4. Zhu, Q.; Guo, Y.; Wang, L.; Liao, C.; Li, F. Improving the Misalignment Tolerance of Wireless Charging System by Optimizing the Compensate Capacitor. *IEEE Trans. Ind. Electron.* **2015**, *62*, 4832–4836. [CrossRef]
5. Baker, T.; NgokoM, Y.; Calasan, R.T. Energy Efficient Cloud Computing Environment via Autonomic Meta-director Framework. In Proceedings of the 2013 Sixth International Conference on Developments in eSystems Engineering (DeSE), Abu Dhabi, UAE, 16–18 December 2013.
6. Baker, T.; Al-Dawsari, B.; Tawfik, H.; Reid, D.; Ngoko, Y. GreeDi: An energy efficient routing algorithm for big data on cloud. *Ad Hoc Netw.* **2015**, *35*, 83–96. [CrossRef]
7. Aldawsari, B.; Baker, T.; England, D. Trusted Energy-Efficient Cloud-Based Services Brokerage Platform. *Int. J. Intell. Comput. Res.* **2015**, *6*, 630–639. [CrossRef]
8. Esteban, B.; Sid-Ahmed, M.; Kar, N.C. A Comparative Study of Power Supply Architectures in Wireless EV Charging Systems. *IEEE Trans. Power Electron.* **2015**, *30*, 6408–6422. [CrossRef]
9. Rush, A.D.; Troyk, P.R. A Power and Data Link for a Wireless-Implanted Neural Recording System. *IEEE Trans. Biomed. Eng.* **2012**, *59*, 3255–3262. [CrossRef] [PubMed]
10. Wang, Z.; Li, Y.; Sun, Y.; Tang, C.; Lv, X. Load Detection Model of Voltage-Fed Inductive Power Transfer System. *IEEE Trans. Power Electron.* **2013**, *28*, 5233–5243. [CrossRef]
11. Ju, X.; Dong, L.; Huang, X.; Liao, X. Switching Technique for Inductive Power Transfer at High-Q Regimes. *IEEE Trans. Ind. Electron.* **2015**, *62*, 2164–2173. [CrossRef]
12. Li, W.; Yuan, H.; Xu, W.; Geng, K.; Wang, G. An Optimization Procedure for Coil Design in a Dual Band Wireless Power and Data Transmission System. *ECS Trans.* **2013**, *52*, 1091–1097. [CrossRef]
13. Wang, G.; Liu, W.L.W.; Sivaprakasam, M.; Zhou, M.; Weiland, J.D.; Humayun, M.S. A Dual Band Wireless Power and Data Telemetry for Retinal Prosthesis. In Proceedings of the International Conference 2006 of the IEEE Engineering in Medicine and Biology Society, New York, NY, USA, 30 August–3 September 2006.
14. Xu, Q.; Hu, D.; Duan, B.; He, J. A Fully Implantable Stimulator with Wireless Power and Data Transmission for Experimental Use in Epidural Spinal Cord Stimulation. *IEEE Trans. Neural Syst. Rehabil.* **2015**, *23*, 683–692. [CrossRef] [PubMed]
15. Kilinc, E.G.; Baj-Rossi, C.; Ghoreishizadeh, S.; Riario, S.; Stradolini, F.; Boero, C.; De Micheli, G.; Maloberti, F.; Carrara, S. A System for Wireless Power Transfer and Data Communication of Long-Term Bio-Monitoring. *IEEE Sens. J.* **2015**, *15*, 6559–6569. [CrossRef]
16. Wang, G.X.; Wang, P.J.; Tang, Y.N.; Liu, W.T. Analysis of Dual Band Power and Data Telemetry for Biomedical Implants. *IEEE Trans. Biomed. Circuits Syst.* **2012**, *6*, 208–215. [CrossRef] [PubMed]
17. Hirai, J.; Kim, T.W.; Kawamura, A. Study on crosstalk in inductive transmission of power and information. *IEEE Trans. Ind. Electron.* **1999**, *46*, 1174–1182. [CrossRef]
18. Wu, J.; Zhao, C.; Lin, Z.; Du, J.; Hu, Y.; He, X. Wireless Power and Data Transfer via a Common Inductive Link Using Frequency Division Multiplexing. *IEEE Trans. Ind. Electron.* **2015**, *62*, 7810–7820. [CrossRef]
19. Yilmaz, G.; Dehollain, C. Single frequency wireless power transfer and full-duplex communication system for intracranial epilepsy monitoring. *Microelectron. J.* **2014**, *45*, 1595–1602. [CrossRef]
20. Yilmaz, G.; Atasoy, O.; Dehollain, C. Wireless Energy and Data Transfer for In-Vivo Epileptic Focus Localization. *IEEE Sens. J.* **2013**, *13*, 4172–4179. [CrossRef]
21. Hirai, J.; Kim, T.W.; Kawamura, A. Integral motor with driver and wireless transmission of power and information for autonomous subspindle drive. *IEEE Trans. Power Electron.* **2000**, *15*, 13–20. [CrossRef]
22. Hirai, J.; Kim, T.-W.; Kawamura, A. Study on intelligent battery charging using inductive transmission of power and information. *IEEE Trans. Power Electron.* **2000**, *15*, 335–345. [CrossRef]
23. Hirai, J.; Tae-Woong, K.; Kawamura, A. Wireless transmission of power and information and information for cableless linear motor drive. *IEEE Trans. Power Electron.* **2000**, *15*, 21–27. [CrossRef]

24. Van Boheemen, E.L.; Boys, J.T.; Covic, G.A. Dual-tuning IPT systems for low bandwidth communications. In Proceedings of the 2007 2nd IEEE Conference on Industrial Electronics and Applications, Harbin, China, 23–25 May 2007.
25. Zhu, Q.; Wang, L.; Guo, Y.; Liao, C.; Li, F. Applying LCC Compensation Network to Dynamic Wireless EV Charging System. *IEEE Trans. Ind. Electron.* **2016**, *63*, 6557–6567. [CrossRef]
26. Li, W.; Zhao, H.; Deng, J.; Li, S.; Mi, C.C. Comparison Study on SS and double-sided LCC compensation topologies for EV/PHEV Wireless Chargers. *IEEE Trans. Veh. Technol.* **2016**, *65*, 4429–4439. [CrossRef]
27. Li, S.; Li, W.; Deng, J.; Nguyen, T.D.; Mi, C.C. A Double-Sided LCC Compensation Network and Its Tuning Method for Wireless Power Transfer. *IEEE Trans. Veh. Technol.* **2015**, *64*, 2261–2273. [CrossRef]
28. Li, W.; Zhao, H.; Li, S.; Deng, J.; Kan, T.; Mi, C.C. Integrated LCC Compensation Topology for Wireless Charger in Electric and Plug-in Electric Vehicles. *IEEE Trans. Ind. Electron.* **2015**, *62*, 4215–4225. [CrossRef]
29. Feng, H.; Cai, T.; Duan, S.; Zhao, J.; Zhang, X.; Chen, C. An LCC-Compensated Resonant Converter Optimized for Robust Reaction to Large Coupling Variation in Dynamic Wireless Power Transfer. *IEEE Trans. Ind. Electron.* **2016**, *63*, 6591–6601. [CrossRef]
30. Zhou, S.; Mi, C.C. Multi-Paralleled LCC Reactive Power Compensation Networks and Their Tuning Method for Electric Vehicle Dynamic Wireless Charging. *IEEE Trans. Ind. Electron.* **2016**, *63*, 6546–6556. [CrossRef]
31. Pantic, Z.; Bai, S.; Lukic, S.M. ZCS LCC-Compensated Resonant Inverter for Inductive-Power-Transfer Application. *IEEE Trans. Ind. Electron.* **2011**, *58*, 3500–3510. [CrossRef]
32. Geng, Y.; Li, B.; Yang, Z.; Lin, F.; Sun, H. A High Efficiency Charging Strategy for a Supercapacitor Using a Wireless Power Transfer System Based on Inductor/Capacitor/Capacitor (LCC) Compensation. *Energies* **2017**, *10*, 10135. [CrossRef]
33. Mai, R.; Chen, Y.; Liu, Y. Compensation Capacitor Alteration Based IPT Battery Charging Application With Constant Current and Constant Voltage Control. In Proceedings of the Chinese Society of Electrical Engineering, Beijing, China, 10–13 August 2016.